From "Smaller is Stronger" to "Size-Independent Strength Plateau": Towards Measuring the Ideal Strength of Iron

Wei-Zhong Han, Ling Huang, Shigenobu Ogata, Hajime Kimizuka, Zhao-Chun Yang, Christopher Weinberger, Qing-Jie Li, Bo-Yu Liu, Xi-Xiang Zhang, Ju Li, Evan Ma, and Zhi-Wei Shan**

The ideal strength of a metal is the stress at which the lattice itself becomes unstable. This property is of practical interest since it sets an upper bound on the strength of a perfect crystal.[1] However, the effect of crystalline imperfections, e.g., the presence of dislocations, renders the strength of metals far less than their ideal strength.[2–5] A straightforward method to increase the strength of a crystal is to reduce or even eliminate its defects and flaws. This can be achieved through increasing the crystal quality[6–9] or reducing the crystal size,[10–13] as revealed by classical experiments on whiskers carried out over half a century ago[7,8] and recent tests on small scale samples.[10–13] Regardless of the methods of how these samples were prepared, the general trend of the size–strength relationship found so far is the same, i.e., "smaller is stronger." For example, the tensile strength of body-centered cubic (bcc) Fe whiskers exhibited strong strengthening behavior along with decreasing sample diameter.[7,8] Despite of the large scatter in the data, the measured tensile strength increased monotonically to ≈13.4 GPa when the sample diameter was reduced to ≈1.6 μm.[7] This stress is very close to the theoretical de-bonding strength of bcc Fe (≈14.2 GPa) based on density functional theory.[14]

Since the measured strength cannot exceed the theoretical strength, based on the trend observed in ref. [7], a size-independent stress plateau should be observed before size-dependent softening[15] begins to take over at room temperature, if we further reduce the sample size. However, no such trend has been reported in past studies. The only exception was for single crystal Mo alloy pillars: Bei et al.[16] found that Mo alloy pillars prepared by chemical etching method yielded without exception at a critical resolved shear stress (τ) of 4.3 GPa for the size regime from 360 to 1000 nm. The size-independent strength was ascribed to the pristine nature of as-synthesized samples. By assuming the validity of the rule of mixtures, the shear modulus (G) of as-synthesized Mo alloy was estimated to be 112 GPa,[16] about 11% lower than that of pure Mo. Nevertheless, τ is only ≈0.038G, about 3 times lower than the ideal shear strength predicted by theoretical calculations.[17] This indicates that pristine samples are a necessary, but not sufficient condition to achieve ideal strength. Consequently, the following questions are still open for discussion: where is the end of "smaller is stronger" trend in terms of sample size? Can the theoretical strength be measured experimentally in free-standing samples? If yes, how can this be realized?

When materials are subjected to external applied stresses, edges, corners, notches, and surface roughness on free surfaces or even atomic-level surface steps can serve as dislocation nucleation sites, at a stress level significantly less than the ideal strength.[18–21] Therefore, in order to experimentally measure the ideal strength in free-standing samples, it is also necessary to suppress surface dislocation nucleation in addition to ensuring pristine internal structure. In principle, a spherical sample with pristine internal structure and passivated smooth surface can be ideal for achieving theoretical strength because

Prof. W.-Z. Han, Dr. L. Huang, Q.-J. Li, B.-Y. Liu, Prof. J. Li, Prof. E. Ma, Prof. Z.-W. Shan
Center for Advancing Materials Performance from the Nanoscale and Hysitron Applied Research Center in China
State Key Laboratory for Mechanical Behavior of Materials
Xi'an Jiaotong University
Xi'an 710049, P. R. China
E-mail: zwshan@mail.xjtu.edu.cn

Prof. S. Ogata, Prof. H. Kimizuka
Department of Mechanical Science and Bioengineering
Osaka University
Osaka 560-8531, Japan

Prof. S. Ogata
Center for Elements Strategy Initiative for Structural Materials
Kyoto University
Kyoto 606-8501, Japan

Prof. Z.-C. Yang
Department of Mechanical Engineering and Materials Science and Department of Bioengineering
University of Pittsburgh
Pittsburgh, PA 15261, USA

Prof. C. Weinberger
Sandia National Laboratories
Albuquerque, NM 87185, USA

Prof. C. Weinberger
Mechanical Engineering and Mechanics Department
Drexel University
Philadelphia, PA 19104, USA

Prof. X.-X. Zhang
Division of Physical Science and Engineering
King Abdullah University of Science & Technology
Thuwal 23955-6900, Saudi Arabia
E-mail: xixiang.zhang@kaust.edu.sa

Prof. J. Li
Department of Nuclear Science and Engineering and Department of Materials Science and Engineering
Massachusetts Institute of Technology
Cambridge, MA 02139, USA

Prof. E. Ma
Department of Materials Science and Engineering
Johns Hopkins University
Baltimore, MD 21218, USA

DOI: 10.1002/adma.201500377

of the following reasons. First, the spherical geometry ensures that the maximum stress site is located inside the sample when it is loaded. This is because, based on classical contact mechanics, when two spherical samples are pushed against each other, the maximum stress is located in the interior of the sample instead of at the contact interface.[22–24] Second, the pristine internal structure will eliminate internal sources for defect nucleation. Third, the passivated smooth surface is expected to effectively reduce or even eliminate the possibility of surface dislocation nucleation. It has been reported that surface coating may suppress surface dislocation nucleation effectively.[25]

In this communication, we choose spherical single crystal iron nanoparticles to investigate the possibility of experimentally measuring ideal strength in free-standing crystals. These nanoparticles were synthesized by argon plasma evaporation of an iron target, and then passivated in a connecting chamber in an inert gas ambient.[26,27] The size of these particles ranged from tens of nanometers to about 500 nm. Transmission electron microscope (TEM) observations found that all these particles have a thin oxidation layer of 4 nm in thickness, regardless of the particle size, exactly the same as that reported before.[26,27] This suggests that these particles are stable in ambient environment. Most of the iron nanoparticles we used have a spherical shape and therefore the significant effect of faceted surface on deformation reported by Mordehai et al.[28] is not important in our test. In addition, the majority of these particles are free of obvious dislocations and geometric defects although the possibility of small defects cannot be ruled out.

In order to measure the strength of individual particles, the nanoparticles were first individually dispersed on a specially designed Si substrate (Figure S1, Supporting Information).[29] In situ compression tests were performed in a JEOL-2100F TEM using a Hysitron PI95 PicoIndenter with a flat diamond punch (diameter ≈1 μm). All the tests were carried out under displacement rate control mode with a constant displacement rate of 5 nm s^{-1}. It was found that single crystal iron particles always experience ultrahigh elastic deformation before yielding. One typical example is shown in **Figure 1**. The outer diameter of this particle is about 200 nm, with a 4 nm γ-Fe_2O_3 shell. The corresponding selected area diffraction pattern (SADP) (inset in Figure 1a) of the nanoparticle confirms its single crystalline nature. During compression, symmetrical contrast contours (marked with white arrow in Figure 1b) were observed to form at the contact interfaces and move forward along with the increase of external applied force until the particle suddenly collapsed (Figure 1b,c). Additional details regarding the

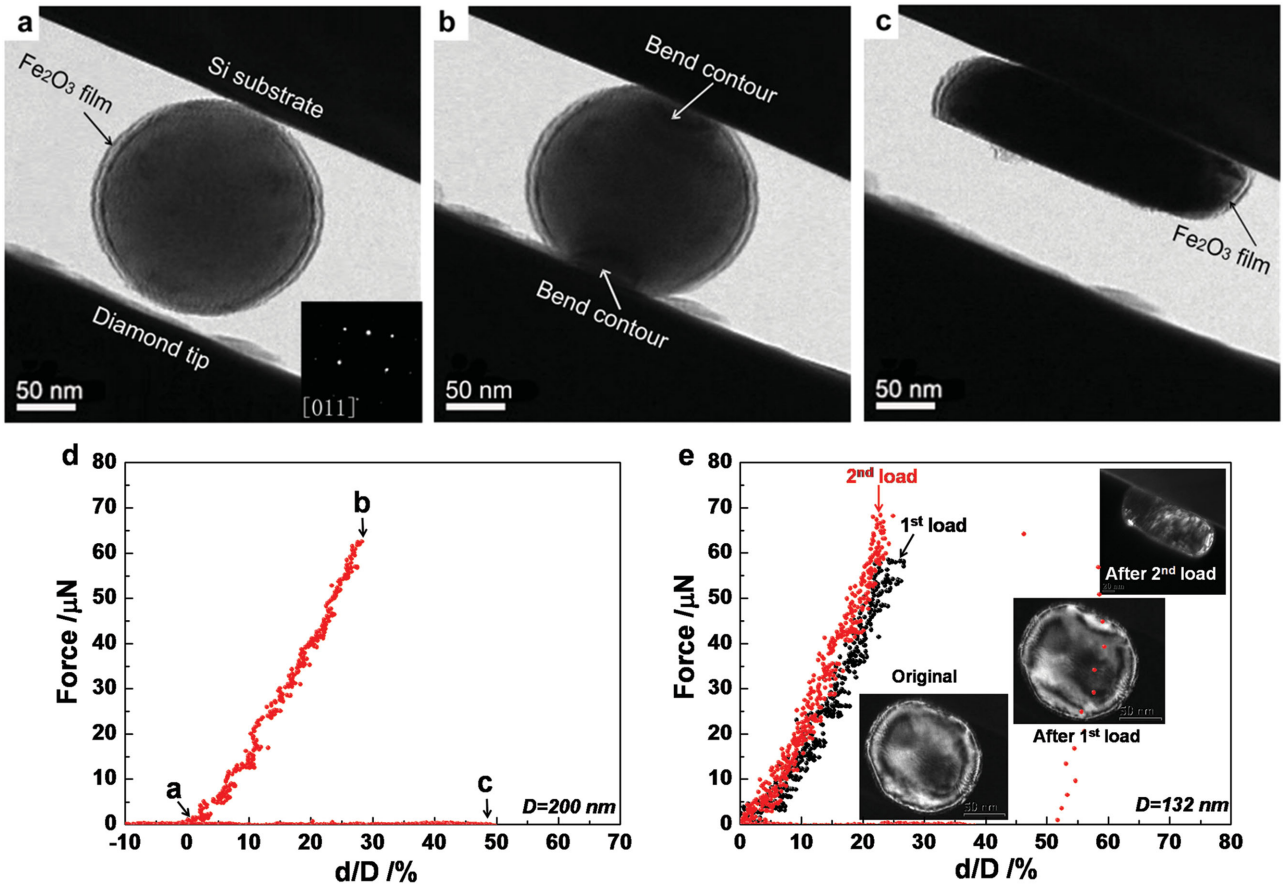

Figure 1. A typical in situ compression test of an individual spherical iron nanoparticle. a–c) Extracted video frames of the in situ compression test of a spherical iron nanoparticles with the diameter of 200 nm. Panels (a,b) are taken at the point marked on the force versus compression strain curves shown in (d). e) The cyclic loading curves of a spherical iron nanoparticles with diameter of 132 nm and the corresponding dark field TEM images before compression, after first loading, and after collapsing.

deformation process are displayed in Movie S1, Supporting Information. During the collapse, the spherical nanoparticle evolved into a pancake-like plate (Figure 1c). This deformation character is significantly different from the compress of nanosphere Si particles, which only demonstrate gradually local surface damage near the contact point and no such catastrophical failure.[30] The recorded force versus compression ratio (defined as the compression displacement divided by the diameter of the nanoparticle) curve exhibited a near linear relationship up to 30%, followed by a sudden load drop (Figure 1d), indicating ultrahigh elastic deformation before the yielding, in agreement with observation of the microstructural evolution. More compression tests on a smaller (75 nm in diameter) and a larger (410 nm in diameter) iron nanospheres were displayed in Movies S2 and S3, Supporting Information, respectively. They all demonstrate similar catastrophic failure feature. In order to confirm the pure elastic deformation before the catastrophic collapse, we unloaded an iron nanoparticle just prior to its plastic yielding and reloaded it to failure. The force versus compression ratio appears quite linear during the first loading sequence (black dots in Figure 1e) with the maximum compression ratio up to 28%. Because we used the "abort" function to unload, no unloading data were recorded during the first loading sequence. However, it is obvious there is no detectable geometry change before (inset of Figure 1e, original) and after (inset of Figure 1e) the first loading sequence. It is worth noting that there was a small movement of this particle during the unloading process due to the adhesion between the sample and the diamond probe. During the second loading sequence, the force versus compression ratio curve nearly overlapped with the first until the sample collapsed at ≈70 μN (Figure 1e, red curve). This suggests that the strain prior to the dramatic collapse is purely elastic. The small discrepancy between the two loading curves as well as the minor contrast difference between the original particle and that after the 1st loading sequence is mainly due to the slight movement of the particle at the end of the first loading sequence.

The collapse process occurred so fast that we can only capture the final state of the particles (e.g., Figure 1c). However, it is interesting to note that the thickness of the deformed iron particles is ≈65 nm (e.g., Figure 1c). This means that the pancake-like iron particles are already a perfect TEM samples and can be easily examined along the thickness direction. In a previous study, we demonstrated that the submicrometer-sized Au particles can experience "pristine to pristine" deformation.[31] In order to examine if iron nanoparticles had experienced a similar process, a Kleindiek nanomanipulator was used to transfer a pancake-like iron particle onto a 3 mm carbon membrane with its flattened surfaces parallel to the membrane (see Figure S2, Supporting Information, for an illustration of the transfer process). As shown in **Figure 2**a, in sharp contrast with that observed in face-centered cubic (FCC) structured Au particles, copious defects are found in the pancake-like iron nanoparticle. The existence of deformation-twinning-like structures (Figure 2b,c) suggests that deformation twinning or local lattice distortion also contributed to the catastrophic plastic evolution. Presumably, this is due to the very high rate of collapse at yielding.[32]

In order to reveal the nucleation and evolution of defects in the nanoparticles, which is beyond the capability of existing

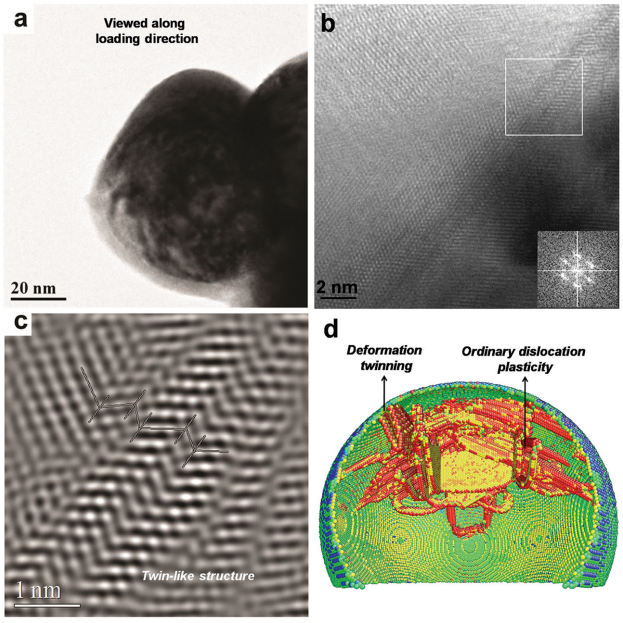

Figure 2. a) TEM image of an iron nanoparticle after plastic deformation viewed along the loading direction. b) High resolution (HR) TEM image of a shear band formed during catastrophic collapsing where multiple deformation twins-like structures are found. The inset shows a fast Fourier transformation (FFT) pattern of this region. c) A Fourier-filtered image from the region marked by the white box in (b). d) MD simulations reveal ordinary dislocation slip and deformation twinning in the deforming iron nanoparticle.

experimental techniques, molecular dynamics (MD) simulations were employed (the details can be found in the Supporting Information). Single crystal iron spheres with diameter of 30 and 60 nm were explored. Regardless of particle size, plenty of defects including dislocations, deformation twins and point defects are observed; they nucleated and interacted with each other and multiplied upon the sudden plastic yielding of the iron particles, leading to the dramatic shape change of the particles in a very short time. Figure 2d is the cross section view of the iron sphere with diameter of 60 nm at the early stage of plastic deformation. Both ordinary dislocation plasticity and deformation twinning are observed to nucleate both from the surface and sample interior and have contributed to the overall plasticity, agreeing well with that observed in laboratory tests.

A total of more than 30 iron nanospheres without obvious flaws were tested in the TEM successfully. Their diameter ranged from 81 to 429 nm. In order to check if the maximum stress sustained by these iron spheres can reach the theoretical strength of iron, we have measured the maximum contact pressure (MCP) of each tested nanosphere and plotted the data versus particle diameter in **Figure 3**. Here MCP is defined as the maximum force sustained by the iron nanosphere prior to the plastic yielding divided by the corresponding contact area, i.e., $\pi d_c^2/4$. Here d_c is the contact diameter corresponding to the maximum force and can be measured directly from the recorded movies. It is worth to point out that Luan and Robbins.[33] had suggested that the continuum contact mechanics will break down when the contact area shrinks into nanoscale. However, the contact area in our experiment is much larger

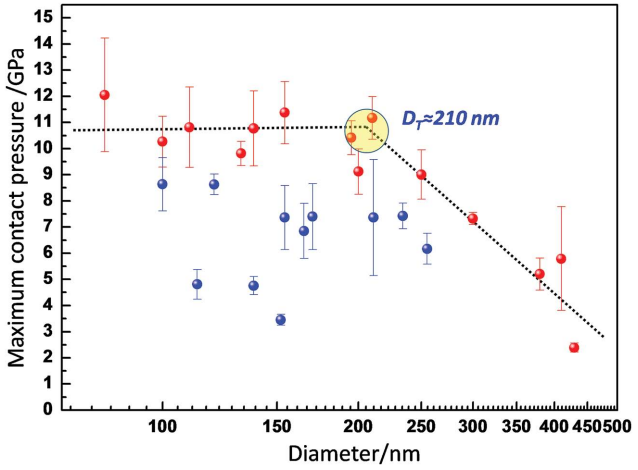

Figure 3. The measured maximum contact pressure as a function of the diameter of spherical iron nanoparticles. A clear size-dependent behavior is found for nanoparticles larger than 210 nm, and a size-independent strength plateau is observed for nanoparticles smaller than 210 nm. The dashed line is added for legibility only.

than their simulation, especially at the point of collapse, and we also observed stress contours predicted by classical theory. It is also worth pointing out that the nascent defects nucleated in MD simulations corresponded to prediction from classical contact theory as well. Therefore the maximum contact pressure computed from a continuum analysis appears to be appropriate to describe the strength of these materials. At first glance, the MCP data appear quite scattered, which is pretty similar to the scatter of whisker's yield strength summarized and modelled by Sudharshan Phani et al.[34] In the current experiments, this scatter is largely due to the following three reasons. First of all, it has been well-established that the strength of single crystal iron has a relatively large orientation dependence. In this study, due to the spherical geometry of the tested samples, the loading orientation must have a distribution, presumably random. Therefore, MCP variation with crystal orientation is expected. Second, even though we have been very careful in carrying out the tests, certain minor misalignments between the samples and the diamond probe as well as the silicon substrate are inevitable. This will also contribute to the scatter of the MCP shown in Figure 3. Third, some defects may be undetectable inside TEM, which can dramatically affect the yield strength of the tested samples. All the aforementioned factors act to scatter the measured MCP, however, they all have the common effect of softening the tested material. In other words, only the highest value found for the MCP of each given sample size represents the condition that is most likely to correspond to the intrinsic strength of the tested samples. Considering these factors, we have purposely highlighted the highest MCP for each sample size in red while all the others in blue, as shown in Figure 3. The data exhibit two obvious size regimes, as marked by the dashed black line. For samples with their diameter larger than ≈210 nm, the size-strengthening behavior agrees with the well-established tenet of "smaller is stronger." However, when the sample diameter is below ≈210 nm, the MCP values (in red color) exhibit a size independent plateau at ≈10.7 GPa, as marked by the horizontal dashed line. It is worth noting that the value of the critical diameter for transition should be closely related to the sample history which will determine the defects state of the samples.[34] Consequently, the critical value for transition may shift back and forth for samples that were fabricated under different conditions. However, the trend for such transition should be same. Based on classical contact mechanics, the maximum stress experienced by an elastically deformed solid sphere should be at a distance underneath the contact surface.[22–24] Therefore, the actual stress causing yielding should be much higher.

In order to obtain a more quantitative assessment of the critical shear stress for yielding, both finite element model (FEM) and interatomic potential finite element model (IPFEM) were employed to analyze the stress distribution in a 210 nm iron sphere just prior to its sudden collapse. As shown in **Figure 4**a, the standard surface to surface contact is defined, and a fine mesh is used to allow more accurate calculation, the effect of crystallographic orientation was considered in our simulation. The force is applied on the top diamond indenter, and the bottom silicon substrate is fixed. The Young's modulus of the 210 nm iron sphere is determined to be about 221 GPa by adjusting the simulated force versus displacement curve to overlap with that measured experimentally (Figure 4b). This value is the isotropic modulus and just in the range of the Young's modulus of bulk single crystal iron, i.e., from 129 to

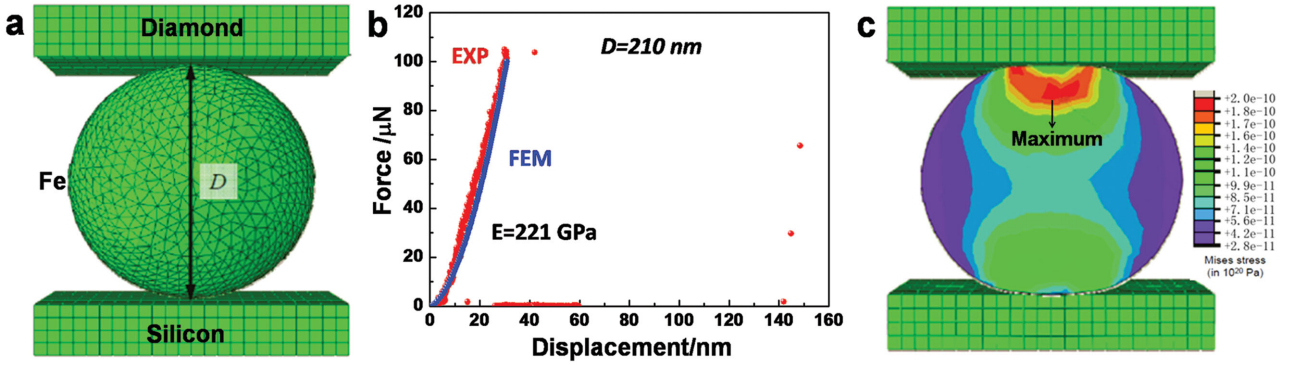

Figure 4. a) The simulation geometry of a compression test of a spherical iron nanoparticle in FEM and IPFEM. b) The estimate of the Young's modulus of an iron spheres with a diameter of 210 nm by using the FEM through direct comparison of the force versus displacement curves. c) Projection of stress on the *x*–*y* plane of the crystal. The color distribution represents the distribution of von Mises stress.

276 GPa, depending on the crystal orientation. One limitation of our FEM is that it can only model linear elastic problems. However, when the external applied stress approaches the theoretical stress of the material, nonlinear elastic deformation has to be considered and anisotropic elasticity must be used to accurately capture stress distributions. We therefore also adopted IPFEM to tackle the nonlinear anisotropic elastic deformation of the 210 nm iron sphere and compressed along ⟨001⟩ orientation. Similar to the stress contour contrast observed during in-situ compression test shown in Figure 1b and Movie S1, Supporting Information, the cross sectional view of the maximum von Mises stress exhibits an arc band profile, as shown in Figure 4c. According to the IPFEM calculation, the corresponding local maximum shear stress on [11–1](101), [11–1](123), and [11–1](112) are 9.4, 12.4, and 12.8 GPa, respectively.

We now compare this stress level with the prediction given by the Frenkel shear model,[35] which gives an estimate of the ideal shear strength of a metal as

$$\tau^{ideal} = \frac{G d_{uvw}}{2\pi d_{hkl}} \quad (1)$$

Where d_{uvw} is the lattice spacing of the shear direction, and d_{hkl} is the lattice spacing of the shear plane, and G is the shear modulus. For bcc single crystal iron, if we use G = 65 GPa as the shear modulus of single crystal iron along the ⟨111⟩ direction,[36] the ideal shear strength is estimated to be 8.45, 14.6, and 22.4 GPa for shear along [11–1](101), [11–1](123), and [11–1](112), respectively. As shown above, our experimental measured data indicate a shear strength of ≈9.4 GPa for [11–1](101) shear. This magnitude is very close to the estimated ideal shear strength of iron by the Frenkel model above and density function theory calculation.[37] In other words, under the triaxial stress loading condition (possible confined pressure effect) and the confinement by the oxide layer in our tests,[22–24,38,39] the upper bound of experimentally measured critical shear stress for yielding is indeed close to the theoretical shear strength of iron.

In summary, our work reveals that the ideal strength can be achieved in the spherical iron nanoparticles with an almost dislocation-free interior. Using quantitative compression in a TEM, we have demonstrated that, when the diameter of iron nanospheres is less than 210 nm or so, the contact pressure saturates at 10.7 GPa, no longer following the usual "smaller is stronger" trend. Structural catastrophic collapse is observed to set in suddenly upon yielding. Microstructural observations and MD simulation found that ordinary dislocation slip and deformation twinning are the dominating plastic deformation mechanisms. Further FEM and IPFEM analysis suggest that the experimentally measured loading pressure/stress plateau corresponds to a maximum shear stress of ≈9.4 GPa, which is very close to the theoretical shear strength of iron for the slip along [11–1](101).

Supporting Information

Supporting Information is available from the Wiley Online Library or from the author.

Acknowledgements

W.-Z.H. and L.H. contributed equally to this work. This work was supported by the grants from NSFC (Grant Nos. 51231005, 51471128, 11132006, and 51321003) and 973 Program of China (2012CB619402). The authors appreciate the support from the 111 Project of China (B06025). W.-Z.H. was supported by the new faculty start-up funding from XJTU. Both E.M. and J.L. carried out this work under an adjunct professorship at XJTU. J.L. acknowledges support by NSF DMR-1120901 and DMR-1240933. S.O. and H.K. acknowledge support by ESISM and JSPS KAKENHI (Grant Nos. 22102003, 23246025, 23109004, 24686072, and 25630013).

Received: January 24, 2015
Revised: March 17, 2015
Published online: April 17, 2015

[1] D. M. Clatterbuck, D. C. Chrzan, J. W. Morris, *Acta Mater.* **2003**, *51*, 2271.
[2] D. M. Dimiduk, D. M. Uchic, T. A. Parthasarathy, *Acta Mater.* **2005**, *53*, 4065.
[3] S. Brinckmann, J. Y. Kim, J. R. Greer, *Phys. Rev. Lett.* **2008**, *100*, 155502.
[4] L. Huang, Q. J. Li, Z. W. Shan, J. Li, J. Sun, E. Ma, *Nat. Commun.* **2011**, *2*, 547.
[5] K. Y. Xie, S. Shrestha, Y. Cao, P. J. Felfer, Y. B. Wang, X. Z. Liao, J. M. Cairney, S. P. Ringer, *Acta Mater.* **2012**, *61*, 439.
[6] H. Bei, S. Shim, G. M. Pharr, E. P. George, *Acta Mater.* **2008**, *56*, 4762.
[7] S. S. Brenner, *J. Appl. Phys.* **1956**, *27*, 1484.
[8] S. S. Brenner, *Science* **1958**, *128*, 569.
[9] G. Richter, K. Hillerich, D. S. Gianola, R. Monig, O. Kraft, C. A. Volkert, *Nano Lett.* **2009**, *9*, 3048.
[10] M. D. Uchic, P. A. Shade, D. M. Dimiduk, *Annu. Rev. Mater. Res.* **2009**, *39*, 361.
[11] O. Kraft, P. A. Gruber, R. Monig, D. Weygand, *Annu. Rev. Mater. Res.* **2010**, *40*, 293.
[12] J. R. Greer, J. T. M. De Hosson, *Prog. Mater. Sci.* **2011**, *56*, 654.
[13] G. Dehm, *Prog. Mater. Sci.* **2009**, *54*, 664.
[14] D. M. Clatterbuck, D. C. Chrzan, J. W. Morris, *Philos. Mag. Lett.* **2002**, *82*, 141.
[15] L. Tian, J. Li, J. Sun, E. Ma, Z. W. Shan, *Sci. Rep.* **2013**, *3*, 2113.
[16] H. Bei, S. Shim, E. P. George, M. K. Miller, E. G. Herbert, G. M. Pharr, *Scr. Mater.* **2007**, *57*, 397.
[17] C. R. Krenn, D. Roundy, J. W. Morris, M. L. Cohen, *Mater. Sci. Eng. A* **2001**, *319*, 111.
[18] L. Zuo, A. H. W. Ngan, G. P. Zheng, *Phys. Rev. Lett.* **2005**, *94*, 095501.
[19] L. Zuo, A. H. W. Ngan, *Philos. Mag. Lett.* **2006**, *86*, 355.
[20] H. Bei, Y. F. Gao, S. Shim, E. P. George, G. M. Pharr, *Phys. Rev. B* **2008**, *77*, 060103.
[21] T. Zhu, J. Li, A. Samanta, A. Leach, K. Gall, *Phys. Rev. Lett.* **2008**, *100*, 025502.
[22] K. L. Johnson, *Contact Mechanics*, Cambridge University Press, Cambridge, **1984**, p. 90.
[23] P. Valentini, W. W. Gerberich, T. Dumitrica, *Phys. Rev. Lett.* **2007**, *99*, 175701.
[24] T. Zhu, J. Li, K. J. Van Vliet, S. Ogata, S. Yip, S. Suresh, *J. Mech. Phys. Solids* **2004**, *52*, 691.
[25] R. Gu, A. H. W. Ngan, *Acta Mater.* **2012**, *60*, 6102.
[26] K. K. Fung, B. Qin, X. X. Zhang, *Mater. Sci. Eng. A* **2000**, *286*, 135.
[27] Y. S. Kwok, X. X. Zhang, B. Qin, K. K. Fung, *Appl. Phys. Lett.* **2000**, *77*, 3971.

[28] D. Mordehai, S. W. Lee, B. Backes, D. J. Srolovitz, W. D. Nix, E. Rabkin, *Acta Mater.* **2011**, *59*, 5202.
[29] Z. W. Shan, R. K. Mishra, S. A. S. Asif, O. L. Warren, A. M. Minor, *Nat. Mater.* **2008**, *7*, 115.
[30] J. D. Nowak, A. R. Beaber, O. Ugurlu, S. L. Girshick, W. W. Gerberich, *Scr. Mater.* **2010**, *62*, 819.
[31] Z. J. Wang, Z. W. Shan, J. Li, J. Sun, E. Ma, *Acta Mater.* **2012**, *60*, 1368.
[32] J. Marian, W. Cai, V. V. Bulatov, *Nat. Mater.* **2004**, *3*, 158.
[33] B. Luan, M. O. Robbins, *Nature* **2005**, *435*, 929.
[34] P. Sudharshan Phani, K. E. Johanns, E. P. George, G. M. Pharr, *Acta Mater.* **2013**, *61*, 2489.
[35] J. Frenkel, *Z. Phys.* **1926**, *37*, 572.
[36] J. A. Rayne, B. S. Chandrasekhar, *Phys. Rev.* **1961**, *122*, 1714.
[37] S. Ogata, J. Li, N. Hirosaki, Y. Shibutani, S. Yip, *Phys. Rev. B* **2004**, *70*, 104104.
[38] D. M. Clatterbuck, D. C. Chrzan, J. W. Morris, *Scr. Mater.* **2003**, *49*, 1007.
[39] W. W. Gerberich, W. M. Mook, C. R. Perrey, C. B. Carter, M. I. Baskes, R. Mukherjee, A. Gidwani, J. Heberlein, P. H. McMurry, S. L. Girshick, *J. Mech. Phys. Solids* **2003**, *51*, 979.